

Coherence and decoherence in quantum absorption refrigerators

Michael Kilgour and Dvira Segal

*Department of Chemistry and Centre for Quantum Information and Quantum Control,
University of Toronto, 80 Saint George St., Toronto, Ontario, Canada M5S 3H6*

(Dated: November 6, 2018)

Absorption refrigerators transfer thermal energy from a cold reservoir to a hot reservoir using input energy from a third, so-called work reservoir. We examine the operation of quantum absorption refrigerators when coherences between eigenstates survive in the steady state limit. In our model, the working medium comprises a discrete, four-level system. We manifest that eigenbasis quantum coherences within this system generally suppress the cooling current in the refrigerator, while minimally affecting the coefficient of performance (cooling efficiency). We rationalize the behavior of the four-level refrigerator by studying two, three-level model systems for energy transport and refrigeration. Our calculations further illuminate the shortcomings of secular quantum master equations, and the necessity of employing dynamical equations of motion that retain couplings between population and coherences.

I. INTRODUCTION

Nanoscale classical and quantum heat machines (QHMs) can be constructed out of few ions¹, atomic-like systems such as natural defects in diamond², and even one atom³, to convert input energy into mechanical, optical, electrical, or thermal work. By utilizing non-classical resources, quantum heat machines may even perform beyond the Carnot limit⁴. Paired with exciting real-world applications, QHMs present a rich playground to investigate fundamental questions at the intersection of thermodynamics and quantum dynamics^{2,5-10}.

Of obvious importance in the study of QHMs are questions over the thermodynamic consistency of the employed open quantum systems methodologies. Typically, projection operator methods are employed in this area^{11,12}, often relying on a perturbative expansion in the system-bath coupling energy, a Markovian (fast-bath) approximation, and the neglect of coherences in the working system through the application of the so-called secular (or “rotating-wave”) approximation. Indeed, it has been shown that certain popular quantum master equation approaches, such as the local-basis Lindblad method, may not respect the laws of thermodynamics, e.g. allowing the heat current to flow against the temperature gradient¹³⁻¹⁷. This issue is vexing enough without considering that it is not generally easy nor necessarily possible to prove that a certain approximate approach will respect thermodynamic laws.

Studies of coherence and decoherence in condensed phases are ubiquitous in the open quantum systems literature. Relevant to our work are the extensive discussions around the role of quantum coherences in energy transfer¹⁸⁻²⁰ and in the operation of QHMs²¹⁻³⁰. For a recent review from a resource theory perspective, see Ref.³¹. Questions around the role of coherences in QHMs and the thermodynamic consistency of methods are in fact intimately linked. For example, global-secular quantum master equation approaches, such as the Gorini-Kossakowski-Lindblad-Sudarshan (GKLS) equation^{11,32}, neglect the effect of coherences on de-

vice operation. Local-secular quantum master equations can re-include some of the effects of coherence, via a change of basis, coming at the cost of strict thermodynamic consistency¹⁵⁻¹⁷. On the other hand, *nonsecular* quantum master equations of the Redfield type¹² cannot in general be guaranteed to provide fully positive populations due to issues concerning initial system-bath correlations³³⁻³⁵, and in general are cumbersome to treat analytically. Furthermore, the Redfield equation may be exercised in the local-site basis, resulting in an improper long-time (equilibrium) state for the system³⁶⁻³⁸.

In this work, we address the interplay of quantum coherences and decoherence processes in an analytically tractable model for a quantum absorption refrigerator (QAR)³⁹. We emphasize that we are considering device operation only in the weak system-bath coupling limit. Performance of strongly-coupled (system-bath) devices is a pursuit of a significant importance, but due to methodological constraints it is outside the scope of the present paper.

A QAR is a continuous-cycle, nondriven heat machine. It extracts energy from a cold reservoir and dumps it to a hot reservoir, assisted by energy absorbed from a so-called work reservoir. The simplest version of such a device, the three-level quantum absorption refrigerator (3IQAR)⁴⁰, has been explored in detail in the weak system-bath coupling limit. Its operating characteristics, such as power and efficiency, are easy to derive when employing Markovian quantum master equations, see e.g. Refs.^{41,42}. Internal system coherences disappear in the 3IQAR in the steady state limit, and the cooling performance can approach the Carnot bound. The basic model and its extensions were recently discussed e.g. in Refs.⁴³⁻⁴⁵. Recent studies on QARs looked at physical realizations⁴⁶, the impact of internal leaks and dissipation⁴⁷, and the roles of topology⁴⁸, internal couplings²⁸, and strong system-bath coupling effects⁴⁹. Other questions of interest include the cooling performance of the QAR at maximum power^{42,50,51}, and the behavior of its current fluctuations⁵².

Here, in order to probe the role of steady state co-

herences in the operation of QARs, we build a four-level quantum absorption refrigerator (4IQAR); in our design, the four-level working fluid is coupled to three thermal reservoirs (work, hot and cold), as well as to an additional, purely decohering bath. This minimal model allows us to interrogate the roles of internal coupling strength, coherence and decoherence in the device operation. Furthermore, using the 4IQAR model we identify and diagnose the shortcomings of secular master equations in the context of QHMs.

To help us understand the operation of the 4IQAR, we analyze two simpler, three-level model systems: the V energy transfer system (VETS) and the 3IQAR. The VETS, a generalization of the well-studied V-system^{53–56}, describes energy exchange between two thermal reservoirs. It will give us insight on methodological issues and the role of coherence in the transport behavior. The 3IQAR forms the basic template for a QAR, which we use to examine the behavior of the more compound 4IQAR.

Previous studies have looked at coherence effects in QHMs, see for example^{21–30}. Here, we provide a rigorous and thorough analysis of the problem within a model system, by studying the interplay between a wide range of internal system couplings and decoherence effects, which largely determine the device performance. Our examination is grounded in a microscopic quantum mechanical equations of motion derived without heuristics. Further, discussions of methodological aptitude of secular master equations have largely focused on problems of energy transport and especially recently, on the local vs. global issue rather than the secular vs. nonsecular problem^{16,17,38}. In our discussion below we address these questions in the context of both energy transfer and heat to work conversion.

Briefly, the central observations of this work are: (i) The presence of steady state coherences in the 4IQAR model degrade the cooling current, but not the efficiency, which in fact is largely unaffected by internal coherences. (ii) The cooling performance of the model can be explained based on the behavior of its building blocks (the VETS and 3IQAR), allowing us to identify key mechanisms in compound models. (iii) The popular secular approximation provides nonphysical predictions for energy transfer and cooling when applied outside its regime of applicability. While this observation is not overly surprising, it emphasizes the importance of a judicious application of open quantum system techniques in the area of quantum thermodynamics.

The paper is organized as follows. We describe the three models, VETS, 3IQAR and 4IQAR in Section II. The performance of these models and possible realizations are presented in Section III; details of the derivations are left to Appendices A-C. We summarize our work in Sec. IV.

II. MODELS

The total Hamiltonian of an open quantum system coupled to multiple (counted by α) reservoirs includes a system Hamiltonian \hat{H}_s , thermal reservoirs \hat{H}_α , and system-bath coupling terms

$$\hat{H} = \hat{H}_s + \sum_{\alpha} \hat{H}_{\alpha} + \sum_{\alpha} \hat{S}_{\alpha} \otimes \hat{B}_{\alpha}. \quad (1)$$

For simplicity, the reservoirs are assumed to comprise collections of independent harmonic oscillators with creation operator $\hat{b}_{q,\alpha}^{\dagger}$ of mode q with frequency $\omega_{q,\alpha}$ in the α bath,

$$\hat{H}_{\alpha} = \sum_q \hbar \omega_{q,\alpha} \hat{b}_{q,\alpha}^{\dagger} \hat{b}_{q,\alpha}. \quad (2)$$

The bath operator \hat{B}_{α} describes displacements of bath oscillators from equilibrium,

$$\hat{B}_{\alpha} = \sum_q \lambda_{q,\alpha} \left(\hat{b}_{q,\alpha}^{\dagger} + \hat{b}_{q,\alpha} \right). \quad (3)$$

\hat{S}_{α} is a system operator, which is system specific. Before studying the 4IQAR, we examine two related, simpler, three-level models. The V energy transfer system describes energy exchange between two heat baths mediated by a three-level quantum system. The three-level QAR operates with null steady state coherences. Using a weak-coupling quantum master equation, we study energy transport and refrigeration in these two models. Equipped with this background, we are able then to rationalize the properties of the four-level QAR.

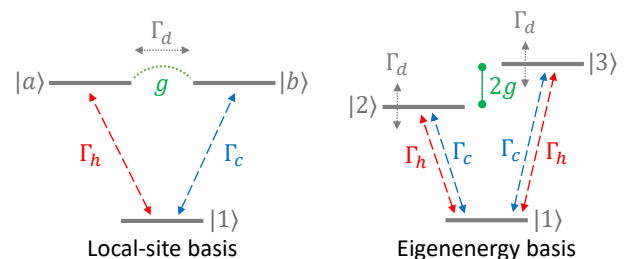


FIG. 1. Diagram of the NEVS in the local site basis (left) and in the energy basis (right). The red and blue arrows represent energy exchange processes with the hot and cold baths, respectively. The gray arrow depicts the effect of the decoherence bath.

A. V energy transfer system

The V and Λ -type systems, with three atomic or molecular levels interacting with coherent or incoherent reservoirs (representing e.g. electromagnetic radiation fields) have been intensively investigated in quantum optics. In

particular, the prospect of generating long-lived coherences in a quantum system has attracted much attention, with applications to lasing, photovoltaic devices and light harvesting systems^{53–56}. While the dynamics of populations and coherences in V and Λ systems has been investigated in detail, so far, few studies considered the nature of energy transport across such systems⁵⁷.

We study the behavior of the V system out of equilibrium in the steady state limit. The model includes three levels and three reservoirs, $\alpha = h, c, d$, see Fig. 1. The hot (h) and cold (c) thermal baths exchange energy—mediated by the system. The so-called dephasing (d) bath is responsible for pure decoherence effects. In the site, “local” basis, the quantum system includes a ground state $|1\rangle$ and two excited states, $|a\rangle$ and $|b\rangle$, which are made degenerate at energy θ . These states are coherently coupled, with a coupling strength g ,

$$\begin{aligned} \hat{H}_s &= \epsilon_1 |1\rangle\langle 1| + \theta (|a\rangle\langle a| + |b\rangle\langle b|) \\ &+ g (|a\rangle\langle b| + |b\rangle\langle a|). \end{aligned} \quad (4)$$

The coupling energy g can be made arbitrarily large. In what follows, we set the reference energy at $\epsilon_1 = 0$. The system \hat{S} operator mediates energy exchange processes and decoherence effects from the environment,

$$\begin{aligned} \hat{S}_h &= |1\rangle\langle a| + h.c., \quad \hat{S}_c = |1\rangle\langle b| + h.c. \\ \hat{S}_d &= |a\rangle\langle b| + h.c. \end{aligned} \quad (5)$$

In the absence of the d bath, energy is transferred between the hot and cold baths as long as $g \neq 0$. In the site basis, we picture energy flow as follows: The hot bath excites the $|a\rangle$ site, which transfers population to the $|b\rangle$ site through the coherent coupling g . Since the population of $|b\rangle$ —relative to the ground state—exceeds the equilibrium value as dictated by the cold bath to which it is coupled, energy is released to the cold bath. Since the excited states are degenerate, the d bath does not provide energy to the system (in the present weak coupling approach). In the system energy basis, the Hamiltonian and the \hat{S}_α operators transform into

$$\hat{H}_s = \epsilon_1 |1\rangle\langle 1| + (\theta - g) |2\rangle\langle 2| + (\theta + g) |3\rangle\langle 3|, \quad (6)$$

and

$$\begin{aligned} \hat{S}_c &= \frac{1}{\sqrt{2}} (|1\rangle\langle 3| - |1\rangle\langle 2| + h.c.) \\ \hat{S}_h &= \frac{1}{\sqrt{2}} (|1\rangle\langle 2| + |1\rangle\langle 3| + h.c.) \\ \hat{S}_d &= |3\rangle\langle 3| - |2\rangle\langle 2|. \end{aligned} \quad (7)$$

In this picture, both excited states are coupled to the ground state via both the hot and cold baths. One may view the model now as having two spins sharing a common ground state, with each spin individually but not independently facilitating energy transfer between the two heat baths. It is also clear now that the d bath is responsible for decoherence, without energy exchange. As we shall see, since both effective spins are coupled to the same heat baths, coherences are generated in the system eigenbasis.

B. Three-level QAR

A simple design of an autonomous quantum absorption refrigerator consists of a three-level system as the working medium and three independent thermal reservoirs^{39,42}, see Fig. 2. Each transition between a pair of levels is coupled to one of the three heat baths, c , h and w , where $T_w > T_h > T_c$. In the steady state limit, the work bath provides energy to the system, allowing the extraction of energy from the cold bath, to be dumped into the hot reservoir. The opposite heating process from the hot bath to the cold can be controlled by manipulating the frequencies of the system. The three-level QAR is described by the system Hamiltonian ($\epsilon_1 = 0$)

$$\hat{H}_s = \theta_c |2\rangle\langle 2| + \theta_h |3\rangle\langle 3|, \quad (8)$$

and we set $\theta_w = \theta_h - \theta_c$. The \hat{S}_α operators are

$$\begin{aligned} \hat{S}_c &= |1\rangle\langle 2| + |2\rangle\langle 1|, \quad \hat{S}_w = |2\rangle\langle 3| + |3\rangle\langle 2| \\ \hat{S}_h &= |1\rangle\langle 3| + |3\rangle\langle 1|. \end{aligned} \quad (9)$$

A decohering bath is not included in this example; as we discuss below in Sec. III, in the weak coupling limit the system’s dynamics is naturally fully secular, with decoupled populations and coherences.

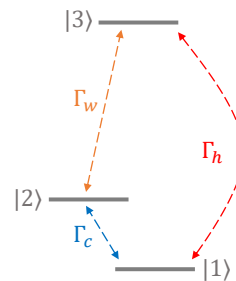


FIG. 2. Diagram of a three-level QAR. The red, blue and orange arrows represent energy exchange processes with the hot, cold and work heat baths.

C. Four-level QAR

The working medium of the 4lQAR comprises four quantum levels. It further includes three heat baths (h , c , w), as well as a decohering bath d , see Fig. 3. In the site basis, the system’s Hamiltonian is

$$\begin{aligned} \hat{H}_s &= \epsilon_1 |1\rangle\langle 1| + \theta_c (|a\rangle\langle a| + |b\rangle\langle b|) + \theta_h |4\rangle\langle 4| \\ &+ g (|a\rangle\langle b| + |b\rangle\langle a|). \end{aligned} \quad (10)$$

We again set the reference energy at $\epsilon_1 = 0$. The system’s operators \hat{S}_α are

$$\begin{aligned} \hat{S}_c &= |1\rangle\langle b| + |b\rangle\langle 1|, \quad \hat{S}_w = |a\rangle\langle 4| + |4\rangle\langle a| \\ \hat{S}_h &= |1\rangle\langle 4| + |4\rangle\langle 1|, \quad \hat{S}_d = |a\rangle\langle b| + |b\rangle\langle a|. \end{aligned} \quad (11)$$

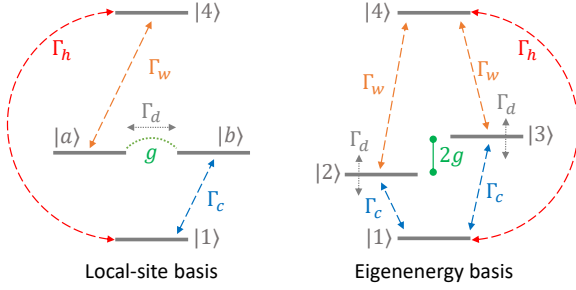


FIG. 3. Diagram of the four-level QAR in the local-site basis (left) and energy basis (right). The red, blue and orange arrows represent energy exchange processes with the hot, cold and work heat baths. The gray arrow shows the effect of the decoherence bath.

After diagonalization we receive

$$\hat{H}_s = (\theta_c - g) |2\rangle\langle 2| + (\theta_c + g) |3\rangle\langle 3| + \theta_h |4\rangle\langle 4|, \quad (12)$$

and

$$\begin{aligned} \hat{S}_c &= \frac{1}{\sqrt{2}} (|1\rangle\langle 3| - |1\rangle\langle 2| + h.c.), \\ \hat{S}_w &= \frac{1}{\sqrt{2}} (|2\rangle\langle 4| + |3\rangle\langle 4| + h.c.) \\ \hat{S}_h &= |1\rangle\langle 4| + |4\rangle\langle 1|, \quad \hat{S}_d = |3\rangle\langle 3| - |2\rangle\langle 2|. \end{aligned} \quad (13)$$

This model is obviously quite complex. Nevertheless, its cooling performance can be explained by studying energy transfer in the VETS model and the cooling behavior of the 3IQAR. A similar model, lacking the dephasing bath, has been explored in the past to address questions of heat leaks and endoreversibility of heat engines⁴⁷. Nevertheless, this study was limited to the secular limit, where

$$\begin{aligned} \dot{\sigma}_{mn}(t) &= -i\omega_{mn}\sigma_{mn}(t) - \sum_{\alpha} \sum_{j,k} \left[R_{mj,jk}^{\alpha}(\omega_{kj})\sigma_{kn}(t) + R_{nk,kj}^{\alpha*}(\omega_{jk})\sigma_{mj}(t) \right. \\ &\quad \left. - [R_{kn,mj}^{\alpha}(\omega_{jm}) + R_{jm,nk}^{\alpha*}(\omega_{kn})]\sigma_{jk}(t) \right]. \end{aligned} \quad (14)$$

Here, $\omega_{mn} = \epsilon_m - \epsilon_n$ are frequencies of the system. The reservoirs act in an additive manner, a direct outcome of the weak system-bath coupling approximation. The dissipation terms in Eq. (14) are

$$\begin{aligned} R_{mn,jk}^{\alpha}(\omega) &= S_{mn}^{\alpha} S_{jk}^{\alpha} \int_0^{\infty} d\tau e^{i\omega\tau} \langle \hat{B}_{\alpha}(\tau) \hat{B}_{\alpha} \rangle \\ &= S_{mn}^{\alpha} S_{jk}^{\alpha} (\Gamma_{\alpha}(\omega) + i\Delta_{\alpha}(\omega)), \end{aligned} \quad (15)$$

with matrix elements $S_{mn}^{\alpha} = \langle m | \hat{S}_{\alpha} | n \rangle$. The average is performed with respect to the canonical thermal state (initial condition) of the α bath. While these R terms, in

populations and coherences are decoupled. In Sec. III we extend this analysis to cover device operation under the combined effects of internal coupling g and coherence effects, while highlighting methodological issues relevant to this setup.

III. METHOD AND RESULTS

We study the system's dynamics using the Redfield equation, a projection operator method¹². This method is derived based on several assumptions: (i) The quantum system weakly couples to its environment, thus the interaction with the different baths is captured within a second order perturbation theory. (ii) The reservoirs are Markovian, and (iii) the initial condition is assumed to be system-bath factorized, with each bath prepared in a canonical thermal state according to its temperature. It is important to note that the Redfield equation in general couples coherences, which are the off diagonal elements of the reduced density matrix (RDM) σ , to populations, the diagonal elements of σ . The Redfield equation is commonly implemented in the system energy basis, though site-basis implementations were also tested. When the inter-site coupling g becomes large, such a local quantum master equation provides an incorrect long time solution, e.g. showing deviations from the thermal equilibrium state^{13,15-17,38}. For a discussion in the context of charge transfer, see for example Refs.^{36,37}.

In the energy basis, the time evolution of σ obeys the following equation of motion¹² in the Schrödinger representation ($\hbar \equiv 1$),

general, are complex numbers, in what follows we neglect the imaginary part Δ since it essentially corresponds to energy shifts. For harmonic baths and bilinear coupling the real part of the dissipator is

$$\Gamma_{\alpha}(\omega) = \begin{cases} \frac{1}{2} J_{\alpha}(\omega) n_{\alpha}(\omega) & \omega < 0 \\ \frac{1}{2} J_{\alpha}(\omega) [n_{\alpha}(\omega) + 1] & \omega > 0. \end{cases} \quad (16)$$

Here, $J_{\alpha}(\omega) = 2\pi \sum_q |\lambda_{q,\alpha}|^2 \delta(\omega_{q,\alpha} - \omega)$ is the spectral density function of the α bath. We assume an ohmic function, $J_{\alpha}(\omega) = \gamma_{\alpha} \omega e^{-|\omega|/\omega_c}$; γ_{α} is a dimensionless interaction parameter. The cutoff frequency ω_c is the largest

energy scale in the problem. $n_\alpha(\omega)$ is the Bose-Einstein occupation function characterized by the temperature of the α bath, $T_\alpha = 1/\beta_\alpha$ ($k_B \equiv 1$). Note that the temperature of the decohering bath d dictates the magnitude of the decoherence rate, yet the d bath does not exchange energy with the system.

While the Redfield equation in general couples the dynamics of populations and coherences, one may invoke the so-called secular approximation and decouple these elements. This approximation can be justified if the natural (coherent) timescale of the system is short relative to its relaxation time—induced by the thermal baths. Furthermore, the equations can be effectively “secularized” if there is strong decoherence process, $\gamma_d \gg \gamma_{h,c,w}$.

In what follows we study the dynamics of the three different models, the VETS, 3IQAR, and 4IQAR by exercising the Redfield equation in the energy basis (diagonal \hat{H}_s). We further compare results to the secularized behavior (whether justified or not), so as to expose the role of coherences. Appendix A includes the full and sec-

ularized Redfield equations for the VETS model, and a discussion over their relative applicability. It should be noted that the Redfield equation is secular by construction for the 3IQAR.

To calculate the energy current we organize the Redfield equation as

$$\dot{\sigma} = -i[\hat{H}_s, \sigma(t)] + \sum_{\alpha} \mathcal{D}_{\alpha} \sigma(t), \quad (17)$$

with the dissipators \mathcal{D}_{α} . In the long time limit, $\dot{\sigma} = 0$, we obtain the steady state solution σ_{ss} . Considering the change of the system’s energy, $d\langle \hat{H}_s \rangle / dt = \text{Tr}[\hat{H}_s \dot{\sigma}]$ (recall that the Hamiltonian does not depend on time) this energy exchange corresponds to heat flow. With that, we get the standard formula for the (steady state) rate of heat exchange with the α reservoir,

$$J_q^{\alpha} = \text{Tr}[\hat{H}_s \mathcal{D}_{\alpha} \sigma_{ss}]. \quad (18)$$

Below we solve equation (14) in the long time limit and find σ_{ss} . We then calculate the heat current from Eq. (18).

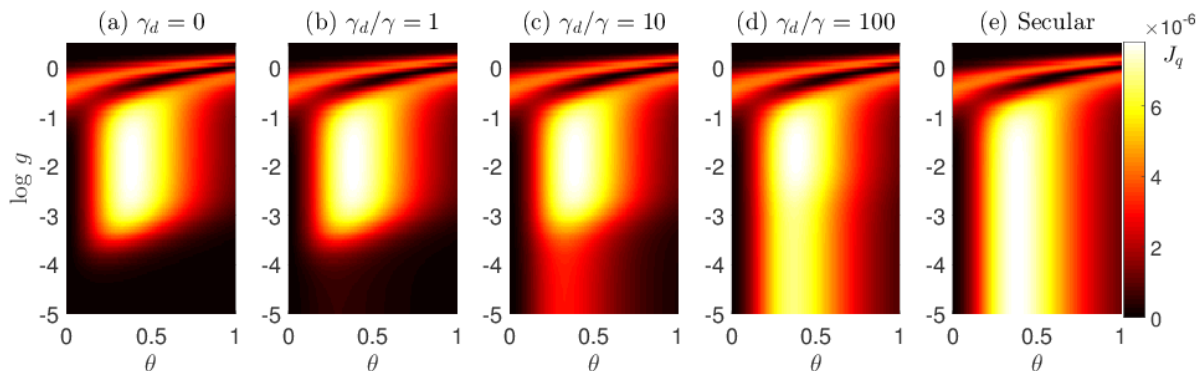


FIG. 4. Heat current in the VETS model. (a)-(d) Solution of the Redfield equation with an increasing decoherence strength between the excited states. (e) When decoherence is sufficiently strong, we retrieve the secular behavior. $\gamma \equiv \gamma_{h,c} = 0.002$, $\omega_c = 50$, $T_h = 0.15$, $T_c = 0.1$, $T_d = 0.12$.

A. Energy flow in the VETS model

The Redfield equation of the VETS model is presented in Appendix A and analytic results for the energy current are derived under the secular approximation. Fig. 4 displays the energy current, from the hot bath to the cold one, as a function of the energy gap θ and the coherent coupling g . We further vary the decoherence rate γ_d throughout panels (a)-(e). The following observations can be made: (i) In the absence of a decohering bath the heat current approaches zero when g becomes very small, which is the expected result. (ii) As we turn on decoherence, the two effective qubits (the pairs 1-2 and 1-3) begin to disentangle from each other. Energy then

flows between the two heat baths even at small g . The large γ_d limit in fact corresponds to the secular behavior, as we show in panel (e). (iii) The energy current is highly non-monotonic as a function of g . (iv) In our parameters, secularization takes place once $\gamma_d > \gamma_{h,c}$. (v) The behavior of the energy current as a function of the spacing θ is intuitive, and it follows trends observed for the spin-boson model⁵⁸: When the gap is small, the energy current increases with θ since more energy is transferred per quantum. However, once we further increase the gap, $\theta \gtrsim 1/\beta_\alpha$, thermal occupation at relevant-resonant frequencies is suppressed, and the heat current rapidly drops.

When coherences are neglected, we are able to reach a

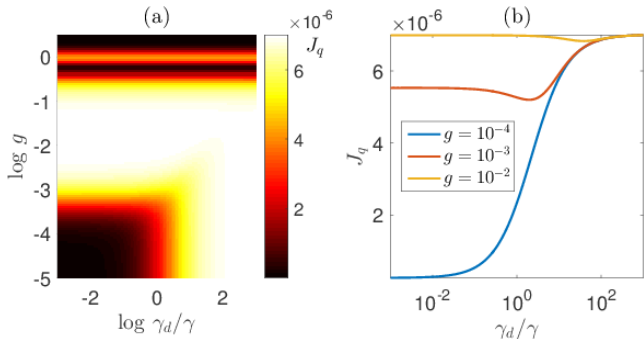


FIG. 5. (a) Contour plot of current in the VETS model as a function of the intersite coupling g and decoherence strength γ_d . (b) Demonstration of a non-monotonic J_q vs. γ_d behavior. $\gamma \equiv \gamma_{h,c} = 0.002$, $\omega_c = 50$, $T_h = 0.15$, $T_c = 0.1$, $T_d = 0.12$, $\theta = 0.5$.

simple closed-form expression for the energy current, see Appendix A for details. In the asymptotic limit of $g \rightarrow 0$ we get

$$J_q = \gamma \theta^2 \frac{n_h(\theta) - n_c(\theta)}{3n_c(\theta) + 3n_h(\theta) + 2}, \quad (19)$$

where $\gamma \equiv \gamma_{h,c}$, and $\gamma_d \gg \gamma$. The current is linear in the coupling parameter γ , as expected from a weak coupling system-bath description. The product of the transferred quantum, which is equal to the transition frequency, by the (ohmic) spectral function leads to the quadratic dependence with θ . Most notably, the current does not vanish at vanishing coupling g . Without the explicit inclusion of γ_d , the nonvanishing current $J_q(g \rightarrow 0) \neq 0$ simply illustrates the breakdown of the secular approximation at small g (panel (e)); in the local-site basis, $J_q(g \rightarrow 0) \rightarrow 0$. Nevertheless, once γ_d is included this finite current is physically attributed to the action of the decohering bath. It couples the $|a\rangle$ and $|b\rangle$ states in the site basis, allowing for energy flow, see Eq. (4).

In Fig. 5 we display the behavior of the current as a function of g and γ_d . Generally, the current increases as we destroy coherences in the system. Nevertheless, we reveal an intriguing regime, with J_q dropping as we increase γ_d . Combining internal couplings with decoherence can therefore impact energy transfer in a highly non-trivial manner.

The behavior of the current as a function of g is quite complex, and we explain it in Figs. 6-7. We further display in Fig. 7 the currents J_q^\pm , calculated separately for each effective spin (of frequency $\theta_\pm = \theta \pm g$). Relevant energy scales in the problems are $\gamma\theta$, which dictates the hot and cold baths-induced decay rates, $\gamma_d\theta$, which determines the decoherence rate, the coherent coupling g , the bare energy θ , the temperatures and the reservoir' cutoff frequency, which is assumed large. In our simulations, $\theta\gamma \ll 1$. Focusing on the $\gamma_d = 0$ case (black line) in Fig. 6, we identify several regimes.

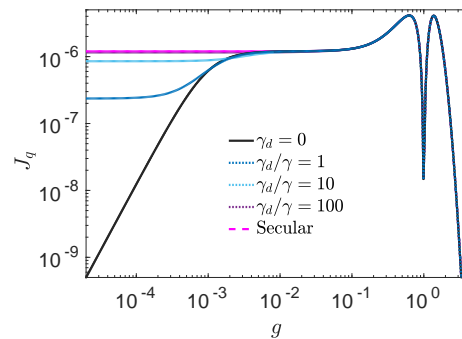


FIG. 6. Heat current in the VETS model as a function of the intersite coupling g . Parameters are the same as in Fig. 4.

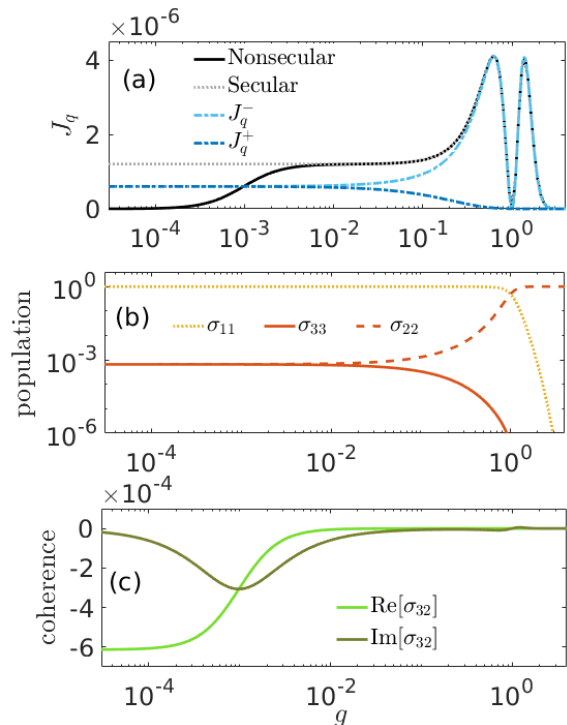


FIG. 7. (a) Current, (b) population and (c) coherences in the VETS model at $\gamma_d = 0$. Parameters are the same as in Fig. 4.

(i) Ultra small coupling, $g \ll \gamma\theta$. In this regime, the heat current follows a quadratic scaling $J_q \propto g^2$. Fig. 7 clearly demonstrates that steady state coherences in the system are responsible for the low- g behavior, which deviates from the secular result. At ultra small g , the population of levels 2 and 3 is essentially equal, and the magnitude of the coherence is significant. (ii) Small coupling regime $g \sim \gamma\theta$. The current grows with g and then it saturates. In parallel, the coherence between the excited states drops to zero, and the populations of levels 2 and 3 begin to deviate. In this regime, $(\theta_+ - \theta_-)/\theta$ grows, eventually justifying the secular approximation. (iii) Intermediate coupling, $\gamma\theta < g < \theta$. The heat current quickly rises—then drops. In this regime, the states

2 and 3 are clearly separated, thus the role of coherence/decoherence is inconsequential. Furthermore, while θ_+ is too large to support energy flow, as it exceeds the thermal energy, heat can be readily transferred between the two baths through the θ_- spin. Nevertheless, once θ_- diminishes, $j_q^- \rightarrow 0$, and the total current is suppressed. (iv) Strong coupling, $\theta < g < 2\theta$. In this regime the V picture does not hold any longer, since the eigenstate $|2\rangle$ lies below $|1\rangle$. Nevertheless, we can study energy flow in the model. We find that as we continue to increase g , the total energy current grows, and it is transferred through the θ_- spin. (v) Ultra strong coupling $g \gg \theta, 1/\beta_\alpha$. The current quickly drops with g since both transitions, θ_\pm , are too large to support heat flow, with the spin gaps exceeding the thermal energy. We confirmed that these trends are general, showing up with other choices of θ and β_α .

The V-type model examined here transfers thermal energy between two heat baths, but it does not operate as a machine since it is missing an additional work source. However, an engine or a cooler can be realized with a V-type model by e.g. periodically driving the transition frequency θ . Such a driven scenario, yet with a perfect degeneracy of excited states in the energy basis, was examined in Ref.³⁰.

B. Four-level QAR with coherences

Equipped with our understanding of energy flow in the VETS, we are ready to examine the operation of quantum absorption refrigerators. In Appendix B, we first review the behavior of the 3IQAR model. As we show below, this model can assist in rationalizing the behavior of the 4IQAR.

We emphasize that in this work we are mostly interested in understanding the cooling performance of the

4IQAR at small g , when internal coherences survive and impact its behavior. Once $g \sim \gamma\theta$, with the internal couplings being comparable to the relaxation rate constants to the heat baths, the system's coherences are lost and the behavior becomes secular. This incoherent-secular situation was nicely explored in Ref.⁴⁷, where different mechanisms responsible for irreversibility in QARs were classified: internal dissipation, which corresponds to the competition between cooling pathways that are optimized at different parameters, and heat leaks, a direct heat exchange between the work and cold baths.

Cooling Current. Based on the Redfield equation, we simulate the system's dynamics and the steady state energy exchange with the different baths. The cooling current of the 4IQAR is presented in Fig. 8, where we display only the cooling region, $J_q^c > 0$. Overall, we observe trends similar to the VETS. First, in panel (a) we show that in the absence of decoherence processes, $\gamma_d = 0$, energy transfer ceases between the states $|a\rangle$ and $|b\rangle$ at small g , and the device cannot function continuously. As we increase the decoherence rate constant in panels (b)-(d), we gradually recapture the secular behavior as depicted in panel (e), with a large cooling current persisting even at vanishing g . The cooling behavior in the 4IQAR is thus analogous to the transport characteristics of the VETS model.

When comparing the cooling current of the 4IQAR to the 3IQAR, one can show analytically that in the secular, low g limit (when the 4IQAR cooling current is observed to be maximal), the 3IQAR outperforms the 4IQAR for any choice of parameters. One can observe this by simple division of Eqs. (B2) and (C4).

We further confirmed (not shown) that the behavior of the cooling current as a function of g and γ_d closely follows trends observed in Fig. 5. This correspondence includes the small domain of non-monotonicity, with the cooling current slightly decreasing with an increase of γ_d at a particular range of g .

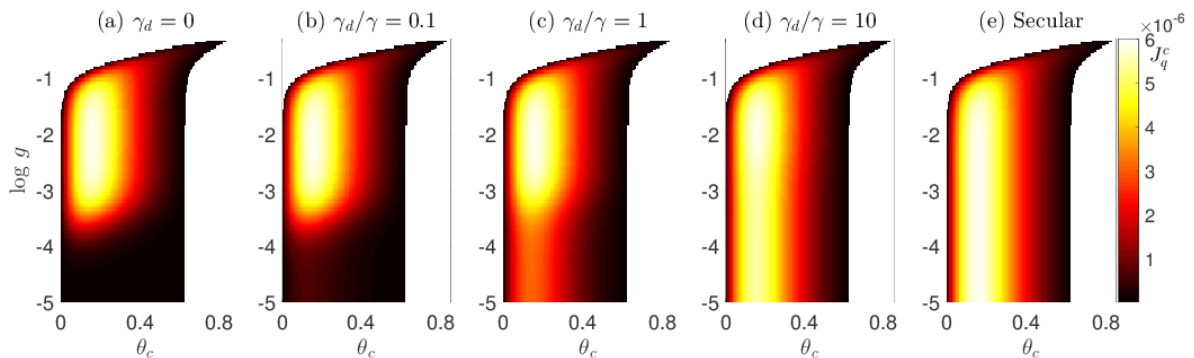


FIG. 8. Cooling current in the 4IQAR. (a)-(d) Solution of the Redfield equation with an increasing decoherence rate between the intermediate states. (e) When γ_d is sufficiently strong, we retrieve the secular behavior. $\gamma \equiv \gamma_{c,h,w} = 0.002$, $\omega_c = 50$, $T_w = 1$, $T_h = 0.15$, $T_c = 0.1$, $T_d = 0.12$, $\theta_h = 1$.

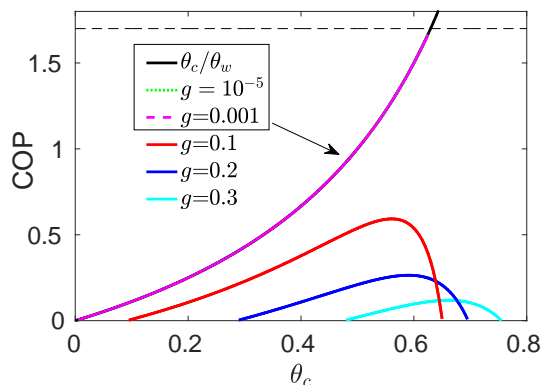


FIG. 9. COP of the 4IQAR for $\gamma_d = 0$ and $\gamma_d/\gamma = 100$ (overlapping). Parameters are the same as in Fig. 8. The dashed line corresponds to the Carnot bound for a cooling machine, $\eta_C = \frac{\beta_h - \beta_w}{\beta_c - \beta_h}$, which equals 1.7 in our parameters.

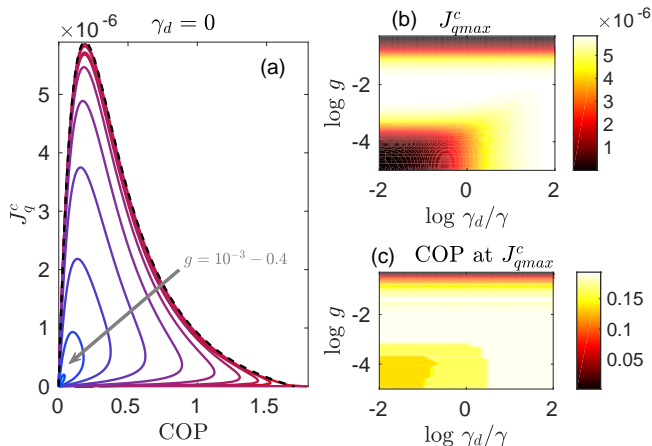


FIG. 10. (a) COP vs. cooling power for the 4IQAR at $\gamma_d = 0$ while increasing g from 10^{-3} to 0.4 as we move inward. The black dashed line corresponds to the secular limit at vanishing g , showing an endoreversible operation. To generate these plots, the frequency θ_c was varied within the cooling window. (b) Maximum cooling current and (c) COP at that value, optimized at every point with respect to θ_c . Parameters are the same as in Fig. 8.

Cooling window. In Appendices B and C, we derive closed-form expressions for the cooling current and cooling condition for the 3IQAR and 4IQAR models respectively—under the secular approximation. In the limit of small g and large γ_d , the cooling window for the 4IQAR model is

$$\frac{\theta_c}{\theta_h} \leq \frac{\beta_h - \beta_w}{\beta_c - \beta_w}, \quad (20)$$

which is identical to the behavior of the 3IQAR. In the parameters of Fig. 8, this “secular” cooling window is defined by $\theta_c < 0.63$. In contrast, when g approaches level spacing, $g \sim \theta_c$, the cooling window of the 4IQAR extends beyond the $\theta_c = 0.63$ bound, as can be seen by

the tail of the cooling window in Fig. 8, developing at large g and large θ_c .

Coefficient of cooling performance. We define the coefficient of cooling performance (COP) as $\eta \equiv J_q^c/J_q^w$, and display it in Fig. 9. In what follows we sometimes refer to the cooling COP as “efficiency”, though it can exceed unity. Unlike the cooling current, we find from simulations that the COP *does not depend on* γ_d . Furthermore, it excellently follows the $\eta = \theta_c/\theta_w$ curve, as long as g is small and $\theta_{c,w}$ are maintained as a meaningful representation of the spacing. When $g = 0.1 - 0.3$ the different cooling pathways, through $\theta_c \pm g$, are differentiated. The behavior in this regime agrees with Ref.⁴⁷

In our model, coherences play an important role in dictating the magnitude of the cooling current. However, the cooling COP largely is independent of internal coherences. In contrast, it is obvious that the efficiency at maximal cooling power depends on the internal coupling g and the decoherence rate constant, as we show in Fig. 10. Our results here agree with⁴⁷. As g increases, the endoreversibility of the engine is lost due to internal dissipation and heat leaks; the refrigerator performance suffers significantly in both power and efficiency, until we exit the cooling window entirely.

In panels (b) and (c) of Fig. 10 we examine the role of decoherence on the performance. Panel (b) illustrates the dramatic damping of the current at low γ_d and g (optimized with respect to θ_c), as observed previously in Fig. 8. Panel (c) displays the COP at maximal cooling current. Since at strong decoherence the cooling behavior of the 4IQAR corresponds to that of the 3IQAR, under the ohmic dissipation the COP at maximal power should be tightly upper bounded by $\eta_C/2$ ^{42,49}, which is about 0.8 in our parameters. Obviously, our parameters are not optimized for performance.

C. Experimental realizations

The energy transfer models described in this work are generic, and may be realized in atomic or molecular systems¹. Moreover, one could envision that the states of the system may represent a coarse grained electronic or excitonic states in nanoscale electronic or amorphous materials. Energy conversion systems were studied in e.g. Refs.^{59,60} based on a classical network picture using a kinetic scheme. Building on this graph method, which is purely classical, we can imagine a network that combines both classical (kinetic) and quantum (coherent) transitions.

The VETS model of Fig. 1 could represent for example a degenerate two-site (termed donor-acceptor) electronic system embedded between two electrodes, see Fig. 11(a). The electrodes are maintained at the same chemical potentials but at different temperatures, T_h and T_c . In this system, carriers transfer energy. The three states in Fig. 1 correspond to empty donor and acceptor sites $|1\rangle \leftrightarrow |00\rangle$, a single electron residing on the donor site

$|a\rangle \leftrightarrow |10\rangle$ and a single electron placed on the acceptor site $|b\rangle \leftrightarrow |01\rangle$. Charge transfer (thus energy flow) between the two metals is driven by the temperature bias, and it proceeds through the coherent tunneling element g . The overall net process can be summarized as follows, $|00\rangle \xrightarrow{\Gamma_h} |10\rangle \xrightarrow{g} |01\rangle \xrightarrow{\Gamma_c} |00\rangle$. Alternatively, one could realize the VETS model with two coherently coupled degenerate qubits that mediate energy flow between two heat baths through their excitation and de-excitation, see e.g. Refs.^{61,62}.

The 3IQAR utilizes input heat from the work reservoir to extract energy from a cold bath. As we show in Fig. 11(b), the model can be realized with a two-site electronic system (or two qubits), similarly to the VETS. However, in the 3IQAR model the donor and acceptor sites are no longer degenerate, with the energy of the donor state placed below the acceptor. As well, in this scenario all transitions are kinetic. The cooling process corresponds to $|00\rangle \xrightarrow{\Gamma_c} |10\rangle \xrightarrow{\Gamma_w} |01\rangle \xrightarrow{\Gamma_h} |00\rangle$.

The 4IQAR can be realized within a photovoltaic cell, with the current flowing between the two metals being assisted by the absorption of solar energy (T_w). The system comprises two degenerate species, donor and acceptor, each represented by a ground state and an excited state (HOMO and LUMO, respectively, in the language of molecular orbitals). We assume that the donor is only coupled to the left (cold) metal, while the acceptor is coupled to the right (hot) lead. Furthermore, the acceptor is excited by the solar energy, allowing energy to flow against the temperature difference. The model is sketched in Fig. 11(c). The four states of the 4IQAR correspond to an empty system $|1\rangle \leftrightarrow |00\rangle$, the donor specie in the HOMO state with an empty acceptor site $|b\rangle \leftrightarrow |\downarrow 0\rangle$, the complementary state with the charge localized on the acceptor site $|a\rangle \leftrightarrow |0\downarrow\rangle$, and the highest energy state, with the acceptor in the excited (LUMO) state $|4\rangle \leftrightarrow |0\uparrow\rangle$. The $|a\rangle$ and $|b\rangle$ states are coherently coupled with a tunneling element g . A cooling process corresponds to the cycle $|00\rangle \xrightarrow{\Gamma_c} |\downarrow 0\rangle \xrightarrow{g} |0\downarrow\rangle \xrightarrow{\Gamma_w} |0\uparrow\rangle \xrightarrow{\Gamma_h} |00\rangle$. Alternatively, the 4IQAR can be realized by three sequential qubits. Excitations transfer coherently between the first two degenerate qubits, and incoherently (assisted by the work bath) between the second and third nondegenerate qubits.

The multi-level models of heat machines explored in this work can therefore represent a variety of devices, such as photovoltaic cells and thermoelectric junctions, while making use of both classical-kinetic and quantum-coherent resources.

IV. SUMMARY

We studied the cooling performance of a generic multi-level QAR with steady state bath-induced coherences. The central observations of this work are the following:

(i) Generally, the presence of coherences in our sys-

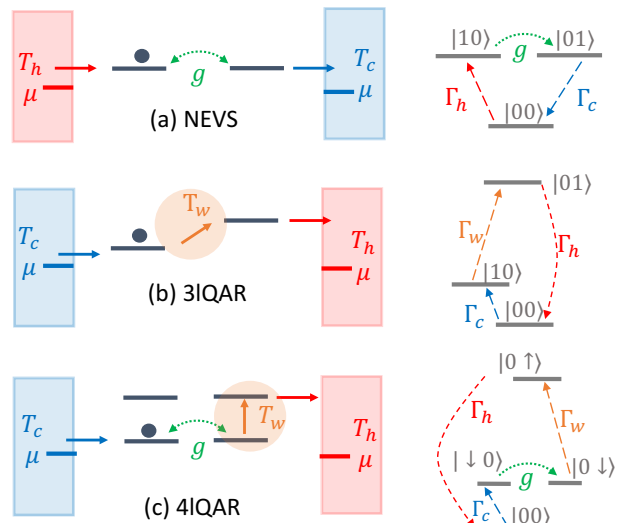


FIG. 11. Schemes of nanoscale energy conversion devices that can be captured with our generic models. (a) The NEVS model can be realized by a conducting junction with two degenerate electronic states. (b) The 3IQAR may correspond to a non-degenerate electronic junction, with the work bath responsible for internal transitions. (c) The 4IQAR can represent a photovoltaic cell. Heat absorbed from the work reservoir is used to transfer carriers—thus energy—from the cold metal to the hot metal. The red, blue and orange arrows represent energy exchange processes with the hot, cold and work heat baths. The effect of the decoherence bath is omitted for simplicity, but it can be further included.

tem degrade the cooling performance of the QAR. Introducing decoherence essentially “secularizes” the coherent dynamics, by suppressing the off-diagonal elements of the reduced density matrix. As a result, at strong decoherence we re-capture the secular dynamics for any internal coupling g . One could interpret this observation by realizing that the survival of coherences in our setup corresponds to state delocalization, which is detrimental to the operation of the QAR. To optimize the performance of our QAR one needs to minimize leaks and internal dissipation (keep g small), while simultaneously minimizing delocalization. This conclusion suggests that in certain designs, strong system-bath coupling effects could enhance performance, by promoting localized dissipation.

(ii) Varying the internal coupling g within the system results in rich behavior as the QAR crosses between different regimes of operation. Moreover, the interplay of internal coupling in the system and decoherence rate reveals a small non-monotonic effect of coherence in the device power.

(iii) The cooling efficiency of the refrigerator, defined as the ratio of extracted heat from the cold bath over input heat from the work reservoir, does not depend on the survival of steady state coherences in the system. In fact, the cooling efficiency of the 4IQAR precisely follows the behavior of the incoherent 3IQAR model when

the internal coupling, g , is small. In contrast, the efficiency at maximal cooling current is quite sensitive to the magnitude of the internal couplings and therefore can be affected and manipulated by internal coherences.

(iv) The Redfield equation, despite its known pathologies regarding positivity, is well-behaved at steady state across a very wide parameter regime explored in this work, and it gives numerical and analytical insight missing in other approaches. The global and local secular quantum master equations catastrophically fail outside their respective regimes of applicability. This fact is not surprising, yet it is important to visualize this failure in the context of QHMs. Specifically, we found that when the global secular equation is applied to a fundamentally nonsecular system it provides erroneous predictions for the cooling current. Nevertheless, our simulations demonstrated that it gives correct results for the cooling COP.

(vi) More generally, our work demonstrates that the operation of a composite quantum heat machine can be explained from the behavior of its components, allowing us to identify key operational principles in energy conversion devices.

Going forward, there are several avenues that should be explored in this area. First, an interesting result of this study which deserves future attention is the insensitivity of the QAR efficiency to coherence/decoherence, in contrast to the quite dramatic effects observed in the current. Future work will examine the connection between efficiency and coherences in QHMs. While we had assessed the system's quantumness by studying its coherences (magnitude of off diagonal elements of the reduced density matrix), it is interesting to further exam-

ine other measures for quantumness and delocalization in quantum energy transport systems and QHMs, such as state purity, inverse participation ratio, entanglement and discord^{6,61,62}.

While quantum thermodynamical machines have been traditionally analyzed under a strict weak-coupling approximation, it is now recognized that to properly characterize the performance of quantum engines and refrigerators, and moreover to achieve new functionality, one must develop methods that are not limited in this respect^{27,49,58,63-73}. The exploration of quantum coherent effects in strongly coupled heat machines is left for future work.

ACKNOWLEDGMENTS

Dvira Segal acknowledges support from an NSERC Discovery Grant and the Canada Research Chair program. The work of Michael Kilgour was supported by an NSERC Canada Graduate Scholarship-Doctoral (CGSD).

APPENDIX A: ENERGY TRANSFER IN THE V SYSTEM

We derive here a closed-form expression for the energy current in the VETS model under the secular approximation. Our starting point is the Redfield equation (14) for the reduced density matrix σ , written in the energy basis ("global Redfield"), which couples the dynamics of populations and coherences. For the VETS model (6)-(7), the Redfield equation reduces to

$$\begin{aligned}
\dot{\sigma}_{11}(t) &= -(R_{12,21} + R_{12,21}^* + R_{13,31} + R_{13,31}^*)\sigma_{11}(t) + (R_{21,12} + R_{21,12}^*)\sigma_{22}(t) + (R_{31,13} + R_{31,13}^*)\sigma_{33}(t) \\
&\quad + (\mathbf{R}_{31,12} + \mathbf{R}_{21,13}^*)\sigma_{23}(t) + (\mathbf{R}_{21,13} + \mathbf{R}_{31,12}^*)\sigma_{32}(t), \\
\dot{\sigma}_{22}(t) &= -(R_{21,12} + R_{21,12}^*)\sigma_{22}(t) + (R_{12,21} + R_{12,21}^*)\sigma_{11}(t) - \mathbf{R}_{21,13}^*\sigma_{23}(t) - \mathbf{R}_{21,13}\sigma_{32}(t), \\
\dot{\sigma}_{33}(t) &= -(R_{31,13} + R_{31,13}^*)\sigma_{33}(t) + (R_{13,31} + R_{13,31}^*)\sigma_{11}(t) - \mathbf{R}_{31,12}\sigma_{23}(t) - \mathbf{R}_{31,12}^*\sigma_{32}(t), \\
\dot{\sigma}_{23}(t) &= +2ig\sigma_{23}(t) - (R_{21,12} + R_{21,12}^*)\sigma_{23}(t) + (\mathbf{R}_{13,21} + \mathbf{R}_{12,31}^*)\sigma_{11}(t) - \mathbf{R}_{31,12}^*\sigma_{22}(t) - \mathbf{R}_{21,13}\sigma_{33}(t) \\
&\quad - (R_{22,22}^d + R_{33,33}^{d,*} - R_{33,22}^d - R_{22,33}^{d,*})\sigma_{23}(t), \\
\dot{\sigma}_{32}(t) &= -2ig\sigma_{32}(t) - (R_{21,12}^* + R_{31,13})\sigma_{32}(t) + (\mathbf{R}_{12,31} + \mathbf{R}_{13,21}^*)\sigma_{11}(t) - \mathbf{R}_{31,12}\sigma_{22}(t) - \mathbf{R}_{21,13}^*\sigma_{33}(t) \\
&\quad - (R_{22,22}^{d,*} + R_{33,33}^d - R_{22,33}^d - R_{33,22}^{d,*})\sigma_{32}(t).
\end{aligned} \tag{A1}$$

For simplicity, we do not explicitly indicate the frequency at which the dissipation elements are calculated, see Eqs. (14)-(15). Note that there are three types of bath-induced terms in Eq. (A1): (i) We put together the rate constants induced by the hot and cold baths, $R_{mn,jk}(\omega) = \sum_{\alpha=h,c} R_{mn,jk}^{\alpha}(\omega)$. For example, $R_{12,21}(\omega) = \Gamma_h(\omega) + \Gamma_c(\omega)$ (ignoring for simplicity the imaginary term). (ii) On top of that, we use

bold faced fonts to highlight terms in which the sum $\sum_{\alpha=h,c} R_{mn,jk}^{\alpha}(\omega)$ turns into the difference between the hot and cold dissipation rates, such as in $R_{21,13}(\omega) = \Gamma_h(\omega) - \Gamma_c(\omega)$. The sign difference develops because the operators \hat{S}_h and \hat{S}_c have opposite signs in front of the transitions $|1\rangle\langle 2| + h.c.$, see Eq. (7). (iii) We separately identify contributions from the decohering bath, for example, $R_{22,22}^d = -R_{22,33}^d = \Gamma_d(0)$. Because $n(0)$ diverges,

the zero-frequency transitions mediated through the decohering bath require some extra effort to compute. In general, this term is dependent on the functional form of the spectral density. For an ohmic bath, we employ L'Hôpital's rule to compute the limit

$$\begin{aligned} J(0)n(0) &= \lim_{\omega \rightarrow 0} \frac{\gamma \omega e^{-|\omega|/\omega_c}}{e^{\beta\omega} - 1} \\ &= \lim_{\omega \rightarrow 0} \frac{\gamma e^{-|\omega|/\omega_c} (\omega_c - \omega)}{\omega_c \beta e^{\beta\omega}} = \frac{\gamma}{\beta}. \end{aligned} \quad (\text{A2})$$

Based on Eq. (A1), we can clearly expose the conditions for which a secular approximation is justified:

(i) Eigenbasis coherences only survive in the long-time limit if the system is driven out of equilibrium, i.e. there is a temperature bias between the reservoirs. If there is no temperature bias, the system will adhere to the Gibbs state defined by the bath temperatures, which is completely diagonal. This can be proved as follows. When $T_h = T_c$, we add up the equations of motion for the coherences, $\dot{\sigma}_{23} + \dot{\sigma}_{32}$, and in the long time limit, we assume zero coherences. The only surviving terms then (in bold) have a sign flip between the two (equal temperature) baths, $\mathbf{R}_{\mathbf{ij},\mathbf{kl}}(\omega_{\mathbf{lk}}) = \Gamma_h(\omega_{\mathbf{lk}}) - \Gamma_c(\omega_{\mathbf{lk}})$. This contribution is proportional to $(\gamma_h - \gamma_c)$, resulting in a trivial identity for the population dynamics. Since the algebraic steady state equation has a unique solution, the trial solution of zero coherences, which does not show contradictions, is valid.

(ii) When g is large compared to the dissipation rate, the so-called ‘‘rotating-wave approximation’’ becomes well-justified. This translates to the timescale of coherence oscillation being short compared to other timescales of the system, and therefore effectively decoupling coherences from the population dynamics.

(iii) Finally, one can directly ‘‘secularize’’ the dynamics by adding strong decoherence effects, $\gamma_d \gg \gamma_{h,c,w}$. This contribution exponentially damps the coherence terms, σ_{23}, σ_{32} , resulting in a secular dynamics.

Working under the secular approximation with population and coherence dynamics decoupled, we find from Eq. (A1) that the populations follow a kinetic equation $|\dot{p}\rangle = \sum_{\alpha=h,c} \mathcal{D}_\alpha |p\rangle$, with the vector $|p\rangle = (p_1, p_2, p_3)^\top$ and the dissipator

$$\mathcal{D}_\alpha = \begin{bmatrix} -k_{1\rightarrow 2}^\alpha - k_{1\rightarrow 3}^\alpha & k_{2\rightarrow 1}^\alpha & k_{3\rightarrow 1}^\alpha \\ k_{1\rightarrow 2}^\alpha & -k_{2\rightarrow 1}^\alpha & 0 \\ k_{1\rightarrow 3}^\alpha & 0 & -k_{3\rightarrow 1}^\alpha \end{bmatrix} \quad (\text{A3})$$

It is useful to define the two relevant frequencies as $\theta_\pm = \theta_\pm g$, see Fig. 1. The rate constants combine two Redfield dissipation rates, for example, $k_{1\rightarrow 2}^h = R_{12,21}^h + R_{12,21}^{h,*}$. Explicitly, they are given by $k_{1\rightarrow 2}^\alpha = \frac{1}{2} J_\alpha(\theta_-) n_\alpha(\theta_-)$ and $k_{1\rightarrow 3}^\alpha = \frac{1}{2} J_\alpha(\theta_+) n_\alpha(\theta_+)$, with the reversed rates $k_{2\rightarrow 1}^\alpha$ and $k_{3\rightarrow 1}^\alpha$ determined from detailed balance. Note, the factor $1/2$ within these expressions results from the $1/\sqrt{2}$ prefactor in front of the eigenbasis operators \hat{S}_α in Eq. (7). Here, $n_\alpha(\theta_\pm) = (e^{\beta_\alpha \theta_\pm} - 1)^{-1}$ is the Bose-Einstein

distribution function and $J_\alpha(\theta_\pm)$ is the spectral density of the α bath. In the ohmic limit with a large cutoff frequency, $\omega_c \gg \theta, g$,

$$k_{1\rightarrow 2}^\alpha = \frac{1}{2} \gamma_\alpha \theta_- n_\alpha^-, \quad k_{1\rightarrow 3}^\alpha = \frac{1}{2} \gamma_\alpha \theta_+ n_\alpha^+, \quad (\text{A4})$$

We use the short notation $n_\alpha^\pm \equiv n_\alpha(\theta_\pm)$. For simplicity, we further assume a symmetric coupling, $\gamma = \gamma_{c,h}$. Recall that $\gamma_{h,c,d}$ are dimensionless coupling parameters.

We readily calculate the energy current (e.g. from the hot bath) using Eq. (18), or directly with the approach described in Ref.⁵², where we construct partial cumulant generating functions. The energy current from the hot bath includes two contributions from the two transitions (‘‘spins’’),

$$\begin{aligned} J_q &= \theta_- \frac{\left[(k_{1\rightarrow 2}^h k_{2\rightarrow 1}^c - k_{1\rightarrow 2}^c k_{2\rightarrow 1}^h) (k_{3\rightarrow 1}^c + k_{3\rightarrow 1}^h) \right]}{\Psi} \\ &+ \theta_+ \frac{\left[(k_{1\rightarrow 3}^h k_{3\rightarrow 1}^c - k_{1\rightarrow 3}^c k_{3\rightarrow 1}^h) (k_{2\rightarrow 1}^c + k_{2\rightarrow 1}^h) \right]}{\Psi}. \end{aligned} \quad (\text{A5})$$

The denominator is

$$\begin{aligned} \Psi &= (k_{1\rightarrow 3}^c + k_{1\rightarrow 3}^h) (k_{2\rightarrow 1}^c + k_{2\rightarrow 1}^h) \\ &+ (k_{3\rightarrow 1}^c + k_{3\rightarrow 1}^h) (k_{2\rightarrow 1}^h + k_{2\rightarrow 1}^c + k_{1\rightarrow 2}^c + k_{1\rightarrow 2}^h). \end{aligned}$$

Equation (A5) describes the energy current in the NEVS model when the population and coherences dynamics are decoupled. The energy current depends on the inter-site coupling g in a rich manner. First, clearly, the frequencies θ_\pm are linear functions in g . More involved behavior arises since the distribution function n_α^\pm further depends on the transition frequency, thus it is a nonlinear function of g .

To the lowest order in g , the levels θ_\pm are degenerate thus $k_{1\rightarrow 2}^\alpha = k_{1\rightarrow 3}^\alpha$. As a result, the current (A5) reduces to

$$J_q = 2\theta \frac{[k_{1\rightarrow 2}^h k_{2\rightarrow 1}^c - k_{1\rightarrow 2}^c k_{2\rightarrow 1}^h]}{2(k_{1\rightarrow 2}^c + k_{1\rightarrow 2}^h) + k_{2\rightarrow 1}^c + k_{2\rightarrow 1}^h}. \quad (\text{A6})$$

Using the concrete expressions for the rate constants (A4), we immediately get

$$J_q = \gamma \theta^2 \frac{n_h(\theta) - n_c(\theta)}{3n_c(\theta) + 3n_h(\theta) + 2}. \quad (\text{A7})$$

Beyond the lowest order in g , corrections are given by a power series, g^{2n} with $n = 1, 2, 3, \dots$. We reiterate that Eq. (A7) is valid when the internal coupling g is small yet the decoherence constant γ_d is large enough such that the secular approximation is well founded.

APPENDIX B: 3LQAR

We derive here an expression for the cooling current in the canonical three-level QAR model. We further discuss

the cooling window and the cooler coefficient of performance (termed efficiency here). In the 3IQAR model, each transition is coupled to a separate thermal bath; internal couplings between system's states are absent. As a result, in this model population and coherences naturally decouple, without the need to further invoke the secular approximation. Using the Redfield equation in a manner analogous to that described in Appendix A, we find that the population dynamics follows a kinetic equation $|\dot{p}\rangle = \sum_{\alpha=c,h,w} \mathcal{D}_\alpha |p\rangle$, with the population vector $|p\rangle = (p_1, p_2, p_3)^\top$, and the total dissipator

$$\sum_\alpha \mathcal{D}_\alpha = \begin{bmatrix} -k_{1\rightarrow 2}^c & k_{2\rightarrow 1}^c & k_{3\rightarrow 1}^h \\ k_{1\rightarrow 2}^c & -k_{2\rightarrow 1}^c - k_{2\rightarrow 3}^w & k_{3\rightarrow 2}^w \\ k_{1\rightarrow 3}^h & k_{2\rightarrow 3}^w & -k_{3\rightarrow 1}^h - k_{3\rightarrow 2}^w \end{bmatrix} \quad (\text{B1})$$

The rate constants for a given transition are given by the Bose-Einstein function and the spectral density, evaluated at the transition frequency, $k_{1\rightarrow 2}^c = J_c(\theta_c)n_c(\theta_c)$, $k_{1\rightarrow 3}^h = J_h(\theta_h)n_h(\theta_h)$ and $k_{2\rightarrow 3}^w = J_w(\theta_w)n_w(\theta_w)$. The reversed rate constants are determined from detailed balance. We assume ohmic spectral functions with large cutoff frequencies. For simplicity, we further take the couplings to be identical at all contacts, $\gamma = \gamma_\alpha$. Since the Bose-Einstein function is evaluated at the transition frequency, we can use the short notation $n_\alpha \equiv n_\alpha(\theta_\alpha)$. Following Eq. (18), the heat current at the c bath is given by

$$J_q^c = \theta_c \frac{k_{1\rightarrow 2}^c k_{2\rightarrow 3}^w k_{3\rightarrow 1}^h - k_{1\rightarrow 3}^h k_{2\rightarrow 1}^c k_{3\rightarrow 2}^w}{\Psi}, \quad (\text{B2})$$

with the denominator

$$\begin{aligned} \Psi &= k_{1\rightarrow 3}^h k_{2\rightarrow 1}^c + k_{1\rightarrow 2}^c k_{2\rightarrow 3}^w + k_{1\rightarrow 3}^h k_{2\rightarrow 3}^w \\ &+ k_{1\rightarrow 2}^c k_{3\rightarrow 1}^h + k_{1\rightarrow 2}^c k_{3\rightarrow 2}^w + k_{1\rightarrow 3}^h k_{3\rightarrow 2}^w \\ &+ k_{2\rightarrow 1}^c k_{3\rightarrow 1}^h + k_{2\rightarrow 1}^c k_{3\rightarrow 2}^w + k_{2\rightarrow 3}^w k_{3\rightarrow 1}^h. \end{aligned} \quad (\text{B3})$$

Explicitly, we find that the cooling current is given by

$$J_q^c \propto \gamma \theta_c [n_c n_w (n_h + 1) - n_h (n_c + 1) (n_w + 1)]. \quad (\text{B4})$$

$$\sum_\alpha \mathcal{D}_\alpha = \begin{bmatrix} -k_{1\rightarrow 2}^c - k_{1\rightarrow 3}^c - k_{1\rightarrow 4}^h & k_{2\rightarrow 1}^c & k_{3\rightarrow 1}^c & k_{4\rightarrow 1}^h \\ k_{1\rightarrow 2}^c & -k_{2\rightarrow 1}^c - k_{2\rightarrow 4}^w & 0 & k_{4\rightarrow 2}^w \\ k_{1\rightarrow 3}^c & 0 & -k_{3\rightarrow 1}^c - k_{3\rightarrow 4}^w & k_{4\rightarrow 3}^w \\ k_{1\rightarrow 4}^h & k_{2\rightarrow 4}^w & k_{3\rightarrow 4}^w & -k_{4\rightarrow 1}^h - k_{4\rightarrow 2}^w - k_{4\rightarrow 3}^w \end{bmatrix} \quad (\text{C1})$$

The rate constants are

$$\begin{aligned} k_{1\rightarrow 2}^c &= \frac{1}{2} J_c(\theta_c^-) n_c(\theta_c^-), & k_{1\rightarrow 3}^c &= \frac{1}{2} J_c(\theta_c^+) n_c(\theta_c^+) \\ k_{2\rightarrow 4}^w &= \frac{1}{2} J_w(\theta_w^+) n_w(\theta_w^+), & k_{3\rightarrow 4}^w &= \frac{1}{2} J_w(\theta_w^-) n_w(\theta_w^-) \\ k_{1\rightarrow 4}^h &= J_h(\theta_h) n_h(\theta_h), \end{aligned} \quad (\text{C2})$$

with the reversed rate constants determined from detailed balance. As in Appendix A, the factor 1/2 results

Positive cooling current, i.e. the extraction of thermal energy from the cold bath, is achieved when the inequality is satisfied,

$$(n_c + 1)(n_w + 1)n_h < (n_h + 1)n_w n_c. \quad (\text{B5})$$

One can then readily identify the cooling window,

$$\frac{\theta_c}{\theta_h} \leq \frac{\beta_h - \beta_w}{\beta_c - \beta_w}. \quad (\text{B6})$$

It can be also shown that the cooling coefficient of performance is

$$\eta \equiv J_q^c / J_q^w = \theta_c / \theta_w, \quad (\text{B7})$$

and that this coefficient is bounded by the Carnot limit,

$$\eta_C = \frac{\beta_h - \beta_w}{\beta_c - \beta_h}. \quad (\text{B8})$$

For the ohmic model, the efficiency at maximal power is tightly bounded by half of the Carnot efficiency⁴².

APPENDIX C: 4LQAR

The 4IQAR combines features from both the NEVS and the 3IQAR. As described in Appendix A, our starting point is the Redfield equation, working as usual in the energy basis. The structure of the equation would be analogous to (A1), with an additional level $|4\rangle$ and the work bath w .

We can easily calculate the cooling current in the 4IQAR model within the secular assumption. First, we define four frequencies, $\theta_c^\pm = \theta_c \pm g$, $\theta_w^\pm = \theta_w \pm g$, which obey $\theta_h = \theta_c^\pm + \theta_w^\mp$. Under the secular approximation, the populations follow a kinetic equation of motion, $|\dot{p}\rangle = \sum_{\alpha=h,c,w} \mathcal{D}_\alpha |p\rangle$, with the population vector $|p\rangle = (p_1, p_2, p_3, p_4)^\top$ and the total dissipator,

using Eq. (18) and get

$$J_q^c = \frac{\theta_c^+}{\Phi} (k_{2 \rightarrow 1}^c + k_{2 \rightarrow 4}^w) (k_{1 \rightarrow 3}^c k_{3 \rightarrow 4}^w k_{4 \rightarrow 1}^h - k_{3 \rightarrow 1}^c k_{4 \rightarrow 3}^w k_{1 \rightarrow 4}^h) \\ + \frac{\theta_c^-}{\Phi} (k_{3 \rightarrow 1}^c + k_{3 \rightarrow 4}^w) (k_{1 \rightarrow 2}^c k_{2 \rightarrow 4}^w k_{4 \rightarrow 1}^h - k_{2 \rightarrow 1}^c k_{4 \rightarrow 2}^w k_{1 \rightarrow 4}^h) \\ - \frac{2g}{\Phi} (k_{1 \rightarrow 2}^c k_{3 \rightarrow 1}^c k_{2 \rightarrow 4}^w k_{4 \rightarrow 3}^w - k_{1 \rightarrow 3}^c k_{2 \rightarrow 1}^c k_{3 \rightarrow 4}^w k_{4 \rightarrow 2}^w). \quad (\text{C3})$$

This expression agrees with Ref.⁴⁷. Here, Φ is a positive normalization factor which is quite cumbersome and has been left out. The first two lines in Eq. (C3) describe heating and cooling processes through the two transitions θ_{\pm} . The last line corresponds to heat leaks, with thermal energy exchanged directly between the work and cold baths. Similarly to the V-system, even in the secular limit the behavior of the energy current is highly non-monotonic in g , affecting the magnitude of cooling current and the cooling window.

Taking $g \rightarrow 0$, the mid-gap states in the 4IQAR model become degenerate and we realize a setup that looks and behaves very much like the 3IQAR. In this limit, the

current reduces to

$$J_q^c = 2\theta_c \frac{k_{1 \rightarrow 2}^c k_{2 \rightarrow 4}^w k_{4 \rightarrow 1}^h - k_{1 \rightarrow 4}^h k_{2 \rightarrow 1}^c k_{4 \rightarrow 2}^w}{\Psi}, \quad (\text{C4})$$

with

$$\Psi = k_{1 \rightarrow 4}^h k_{2 \rightarrow 1}^c + 2k_{1 \rightarrow 2}^c k_{2 \rightarrow 4}^w + 2k_{1 \rightarrow 2}^c k_{4 \rightarrow 1}^h + k_{1 \rightarrow 4}^h k_{2 \rightarrow 4}^w \\ + k_{2 \rightarrow 1}^c k_{4 \rightarrow 1}^h + 4k_{1 \rightarrow 2}^c k_{4 \rightarrow 2}^w + 2k_{1 \rightarrow 4}^h k_{4 \rightarrow 2}^w \\ + 2k_{2 \rightarrow 1}^c k_{4 \rightarrow 2}^w + k_{2 \rightarrow 4}^w k_{4 \rightarrow 1}^h. \quad (\text{C5})$$

This result is analogous to the current for the 3IQAR, Eq. (B2)—with a different denominator (normalization factor), and a factor of 2 here, accounting for the two effective cycles. Note that level ‘3’ in the 3IQAR model serves as level ‘4’ in the 4IQAR model. Also note that the rate constants defined for the 4IQAR are half the value of the rate constants defined for the 3IQAR.

In this $g \rightarrow 0$ and large γ_d limit, we find that the cooling current of the 4IQAR, Eq. (C4), is smaller than the one for the 3IQAR, Eq. (B2), but the cooling window is identical, Eq. (B6). One can similarly calculate the thermal energy absorbed from the work bath, J_q^w , and find that it follows Eq. (C4), only with the energy prefactor θ_w . Thus, when $g \rightarrow 0$ and γ_d is large, the coefficient of performance for the 4IQAR is identical to that of the 3IQAR, $\eta = \theta_c/\theta_w$.

-
- ¹ G. Maslennikov, *et al.*, arXiv:1702.08672.
² J. Klatzow, *et al.*, arXiv:1710.08716v2.
³ J. Roßnagel, *et al.*, S. T. Dawkins, K. N. Tolazzi, O. Abah, E. Lutz, F. Schmidt-Kaler and K. Singer, *Science* **352**, 325 (2016).
⁴ J. Klaers, S. Faelt, A. Imamoglu and E. Togan, *Phys. Rev. X* **7**, 031044 (2017).
⁵ R. Kosloff, *Entropy* **15**, 2100 (2013).
⁶ J. Goold, M. Huber, A. Riera, L. del Rio and P. Skrzypczyk, *J. Phys. A: Math. Theor.* **49**, 143001 (2016).
⁷ S. Vinjanampathy and J. Anders, *Contemporary Physics* **57**, 1 Taylor and Francis (2016).
⁸ R. Alicki and R. Kosloff, arXiv:1801.08314.
⁹ A. Ghosh, V. Mukherjee, W. Niedenzu and G. Kurizki, arXiv:1804.05659
¹⁰ A. Ghosh, V. Mukherjee, W. Niedenzu
¹¹ H.-P. Breuer and F. Petruccione, *The Theory of Open Quantum Systems*, Oxford University Press, New York 2002.
¹² A. Nitzan, *Chemical Dynamics in Condensed Phases: Relaxation, Transfer and Reactions in Condensed Molecular Systems*, Oxford University Press, UK 2006.
¹³ H. Wichterich, M. J. Henrich, H.-P. Breuer, J. Gemmer and M. Michel, *Phys. Rev. E* **76**, 031115 (2007).
¹⁴ L.-A. Wu and D. Segal, *J. Phys. A: Math. and Theo.* **42**, 025302 (2009).
¹⁵ A. Levy and R. Kosloff, *Europhys. Lett.* **107**, 20004 (2014).
¹⁶ P. P. Hofer, M. Perarnau-Llobet, P. D. M. Miranda, G. Haack, R. Silva, J. B. Brask and N. Brunner, *New J. Phys.* **19**, 123037 (2017).
¹⁷ J. O. Gonzalez, L. A. Correa, G. Nocerino, J. P. Palao, D. Alonso and G. Adesso, *Open Syst. Inf. Dyn.* **24**, 1740010 (2017).
¹⁸ A. Chenu and G. D. Scholes, *Annu. Rev. Phys. Chem.* **66**, 69 (2015), and references therein.
¹⁹ H. G. Duan, *et al.*, *Proc. Nat. Acad. Sci.* **32**, 8493 (2017).
²⁰ G.D. Scholes, *et al.*, *Nature* **543**, 647 (2017).
²¹ M. O. Scully, *Phys. Rev. Lett.* **104**, 207701 (2010).
²² M. O. Scully, K. R. Chapin, K. E. Dorfman, M. B. Kim and A. Svidzinsky, *Proc. Nat. Acad. Sci. USA* **108**, 15097 (2011).
²³ K. E. Dorfman, D. V. Voronine, S. Mukamel and M. O. Scully, *Proc. Nat. Acad. Sci. USA* **110**, 2746 (2013).
²⁴ C. Creatoro, M. A. Paeker, S. Emmott and A. W. Chin, *Phys. Rev. Lett.* **111**, 253601 (2013).
²⁵ R. Uzdin, *Phys. Rev. Appl.* **6**, 024004 (2016).
²⁶ R. Uzdin, A. Levy and R. Kosloff, *Entropy* **18**, 124 (2016).
²⁷ K. E. Dorfman, D. Xu and J. Cao, *Phys. Rev. E* **97**, 042120 (2018).
²⁸ S. Seah, S. Nimmrichter and V. Scarani, arXiv:1803.02002.
²⁹ J.-Y. Du and F.-. Zhang, arXiv:1707.07295.
³⁰ W. Niedenzu, D. Gelbwaser-Kilmovsky and G. Kurizki, *Phys. Rev. E* **92**, 042123 (2015).
³¹ A. Streltsov, G. Adesso and M. B. Plenio, *Rev. Mod. Phys.* **89**, 041003 (2017).
³² D. Chruscinski and S. Pascazio, *Open Syst. Inf. Dyn.* **24**, 1740001, (2017).
³³ S. Gnutzmann and F. Haake, *Z. Phys. B.* **101**, 263 (1996).
³⁴ A. Suarez, R. Silbey and I. Oppenheim, *J. Chem. Phys.* **97**, 5101 (1992).
³⁵ P. Pechukas, *Phys. Rev. Lett.* **73**, 8 (1994).
³⁶ R. A. Harris and R. J. Silbey, *J. Chem. Phys.* **83**, 1069

- (1985).
- ³⁷ D. Segal, A. Nitzan, W. B. Davis, M. R. Wasielewski and M. A. Ratner, *J. Phys. Chem. B.* **104**, 3817 (2000).
- ³⁸ A. Purkayastha, A. Dhar and M. Kulkarni, *Phys. Rev. A* **93**, 062114 (2016).
- ³⁹ R. Kosloff and A. Levy, *Ann. Rev. Phys. Chem.* **65**, 365 (2014).
- ⁴⁰ H. E. D Scovil and E. O. Schulz-DuBois, *Phys. Rev. Lett.* **2**, 262 (2012).
- ⁴¹ A. Levy and R. Kosloff, *Phys. Rev. Lett.* **108**, 070604 (2012).
- ⁴² L. A. Correa, J. P. Palao, D. Alonso and G. Adesso, *Sci. Rep.* **4**, 3949 (2014).
- ⁴³ N. Linden, S. Popescu and P. Skrzypczyk, *Phys. Rev. Lett.* **105**, 130401 (2010).
- ⁴⁴ P. Skrzypczyk, N. Brunner, N. Linden and S. Popescu, *J. Phys. A: Math. Theo.* **44**, 492002 (2011).
- ⁴⁵ N. Brunner, N. Linden, S. Popescu and P. Skrzypczyk, *Phys. Rev. E* **85**, 051117 (2012).
- ⁴⁶ M. T. Mitchison, M. Huber, J. Prior, M. P. Woods and M. B. Plenio, *Quantum Sci. Technol.* **1**, 015001 (2016).
- ⁴⁷ L. A. Correa, J. P. Palao and D. Alonso, *Phys. Rev. E* **92**, 032136 (2015).
- ⁴⁸ J. O. Gonzalez, J. P. Palao and D. Alonso, *New J. Phys.* **19**, 113037 (2017).
- ⁴⁹ A. Mu, B. K. Agarwalla, G. Schaller and D. Segal, *New J. Phys.* **19**, 123034 (2017).
- ⁵⁰ L. A. Correa, J. P. Palao, C. Adesso and D. Alonso, *Phys. Rev. E* **87**, 042131 (2013).
- ⁵¹ L. A. Correa, J. P. Palao, G. Adesso and D. Alonso, *Phys. Rev. E* **90**, 062124 (2014).
- ⁵² D. Segal, e-print arXiv:1803.03713
- ⁵³ V. V. Kozlov, Y. Rostovtsev and M. O. Scully, *Phys. Rev. A* **74**, 063829 (2006).
- ⁵⁴ T. V. Tscherbul and P. Brumer, *Phys. Rev. Lett.* **113**, 113601 (2014).
- ⁵⁵ T. V. Tscherbul and P. Brumer, *J. Chem. Phys.* **142**, 104107 (2015).
- ⁵⁶ A. Dodin, T. Tscherbul and P. Brumer, *J. Chem. Phys.* **144**, 244108 (2016).
- ⁵⁷ J. Jing, D. Segal, B. Li and L.-A. Wu, *Scientific Reports* **5**, 15332 (2015).
- ⁵⁸ N. Boudjada and D. Segal, *J. Phys. Chem. A* **118**, 11323 (2014).
- ⁵⁹ M. Einax and A. Nitzan, *J. Phys. Chem. C* **118**, 27226 (2014).
- ⁶⁰ M. Einax and A. Nitzan, *J. Chem. Phys.* **145**, 014108 (2016).
- ⁶¹ L.-A. Wu and D. Segal, *Phys. Rev. A* **84**, 012319 (2011).
- ⁶² A. Kato and Y. Tanimura, *J. Chem. Phys.* **143**, 064107 (2015).
- ⁶³ D. Gelbwaser-Klimovsky and A. Aspuru-Guzik, *J. Phys. Chem. Lett.* **6**, 3477 (2015).
- ⁶⁴ G. Katz and R. Kosloff, *Entropy* **18**, 186 (2016).
- ⁶⁵ D. Xu, C. Wang, Y. Zhao and J. Cao, *New J. Phys.* **18**, 023003 (2016).
- ⁶⁶ P. Strasberg, G. Schaller, N. Lambert and T. Brandes, *New J. Phys.* **18**, 073007 (2016).
- ⁶⁷ A. Kato and Y. Tanimura, *J. Chem. Phys.* **145**, 224105 (2016).
- ⁶⁸ C. Jarzynski, *Phys. Rev. X* **7**, 011008 (2017).
- ⁶⁹ P. Strasberg and M. Esposito, *Phys. Rev. E* **95**, 062101 (2017).
- ⁷⁰ D. Newman, F. Mintert and A. Nazir, *Phys. Rev. E* **95**, 032139 (2017).
- ⁷¹ G. Giusteri, F. Recrosi, G. Schaller and G. L. Celardo, *Phys. Rev. E* **96**, 012113 (2017).
- ⁷² H. M. Friedman, B. K. Agarwalla and D. Segal, e-print arXiv:1802.00511.
- ⁷³ A. Kato and Y. Tanimura, arXiv:1804.02157.